Article:
Raju, K., Wheatcroft, L., Lai, M.C. et al. (2024) Influence of cathode calendering density on the cycling stability of Li-Ion batteries using NMC811 single or poly crystalline particles. Journal of The Electrochemical Society, 171 (8). 080519. ISSN: 0013-4651

https://doi.org/10.1149/1945-7111/ad6378

OPEN ACCESS

Influence of Cathode Calendering Density on the Cycling Stability of Li-Ion Batteries Using NMC811 Single or Poly Crystalline Particles

To cite this article: Kumar Raju *et al* 2024 *J. Electrochem. Soc.* **171** 080519

Journal of The Electrochemical Society, 2024 **171** 080519

Influence of Cathode Calendering Density on the Cycling Stability of Li-Ion Batteries Using NMC811 Single or Poly Crystalline Particles

Kumar Raju,[1,2,z] Laura Wheatcroft,[2,3] May Ching Lai,[2,4] Amoghavarsha Mahadevegowda,[2,4] Louis F. J. Piper,[2,5] Caterina Ducati,[2,4] Beverley J. Inkson,[2,3] and Michael De Volder[1,2,z]

[1]*Institute for Manufacturing, Department of Engineering, University of Cambridge, CB3 0FS, Cambridge, United Kingdom*
[2]*The Faraday Institution, Harwell Science and Innovation Campus, Didcot OX11 0RA, United Kingdom*
[3]*Department of Materials Science and Engineering, University of Sheffield, Sheffield, S1 3JD, United Kingdom*
[4]*Department of Materials Science and Metallurgy, University of Cambridge, Cambridge CB3 0FS, United Kingdom*
[5]*WMG, University of Warwick, Coventry, CV4 7AL, United Kingdom*

Calendering of battery electrodes is a commonly used manufacturing process that enhances electrode packing density and therefore improves the volumetric energy density. While calendering is standard industrial practice, it is known to crack cathode particles, thereby increasing the electrode surface area. The latter is particularly problematic for new Ni-rich layered transition metal oxide cathodes, such as NMC811, which are known to have substantial surface-driven degradation processes. To establish appropriate calendering practices for these new cathode materials, we conducted a comparative analysis of uncalendered electrodes with electrodes that have a 35% porosity (industrial standard), and 25% porosity (highly calendered) for both single crystal (SC) and polycrystalline (PC) NMC811. PC cathodes show clear signs of cracking and decrease in rate capability when calendered to 25% porosity, whereas SC NMC811 cathodes, achieve better cycling stability and no penalty in rate performance at these high packing densities. These findings suggest that SC NMC811 cathodes should be calendered more densely, and we provide a comprehensive overview of both electrochemical and material characterisation methods that corroborate why PC and SC electrodes show such different degradation behaviour. Overall, this work is important because it shows how new single-crystal cathode materials can offer additional advantages both in terms of rate performance and cycling stability by calendaring them more densely.
 [DOI: 10.1149/1945-7111/ad6378]

Manuscript submitted May 10, 2024; revised manuscript received June 18, 2024. Published August 14, 2024.

Supplementary material for this article is available online

In order to reduce our reliance on cobalt (Co), which is expensive and has issues related to sustainability and mining ethics,[1] next-generation lithium-ion batteries (LIBs) for Electric vehicles (EVs), favour the use of Ni-rich cathodes such as NMC811. In addition, these batteries offer higher gravimetric energy densities, which reach up to approximately 250 Wh kg^{-1} in commercial batteries.[2,3] In order to also achieve high volumetric energy densities, electrodes require calendering, which is a standard industrial process where electrodes are passed through rollers that compress the electrode and pack more active material per unit volume.[4,5]

Calendering is known to improve the electrical conductivity of electrodes by creating a better electric contact between the electrode components.[6,7] In addition, it has been suggested that this enhanced interfacial contact between the electrode components helps prevent the disconnection of carbon and active particles, resulting in reduced polarization over time and improved rate capability and cycle life.[8–14] However, the increased energy density usually comes at the expense of rate capability due to the limitation in ion transport when electrode pores become smaller, and therefore the calendering density needs to be selected judiciously depending on the power and energy requirements of the application.[15,16] Another challenge to take into account is that calendering has been shown to crack cathode particles, which increases the active material surface area and might accelerate battery degradation processes.[8,17,18] In particular, Ni-rich cathodes such as NMC811 are known to suffer from surface-driven degradation processes,[19–21] which require further investigation of the optimal calendering density for these advanced cathodes.

When studying the calendering of NMC811 cathodes, it is important to make a distinction between poly-crystalline (PC) cathodes consisting of sintered sub-micrometre primary particles and grain boundary-free single crystal (SC) particles. The latter shows higher resistance to cracking under mechanical load and therefore might withstand high calendering conditions better.[22–28]

This work seeks to increase the energy density of single crystal cathode materials by calendering to higher electrode densities without affecting battery lifetime. We have investigated the performance of polycrystalline and single-crystal NMC811 electrodes under different calendering conditions, including their cracking, volumetric capacity, and cycle stability. Specifically, we compare uncalendered electrodes with ones calendered to 35% porosity (a typical industrial value) and 25% porosity (highly calendered). Our findings demonstrate that for PC NMC811, a calendaring density of 35% offers a good compromise between energy density, rate performance and lifetime. However, SC NMC811 electrodes can be calendered to 25% porosity without suffering penalties in rate capability or cycle stability. In fact, cycling stability is improved at these high packing densities. On the other hand, polycrystalline cathodes calendered to 25% porosity showed a higher degree of cracking and poor rate performance. In this paper, we analyse the origins of this difference in calendaring behaviour, which may offer further advantages to using single crystal compared to polycrystalline cathode materials.

Results and Discussion

The electrode structures in Fig. 1a depict schematically the particle arrangements in uncalendered electrodes and ones calendered to 35% and 25% porosity. Optical images of SC NMC811 cathode cross sections are shown in Fig. 1b, which demonstrates the reduction of electrode thickness that calendering can achieve by increasing the packing density. The SC electrode was calendered from its initial thickness of 100 μm (43% porosity) to 80 μm and 70 μm to get 35% and 25% porosity, whereas the PC electrode was calendered from 115 μm to 90 μm and 80 μm. Charge-discharge profiles of polycrystalline and single-crystal electrodes with different calendering porosity are shown in Fig. S1 and demonstrate that this

[z]E-mail: kr516@cam.ac.uk; mfld2@cam.ac.uk

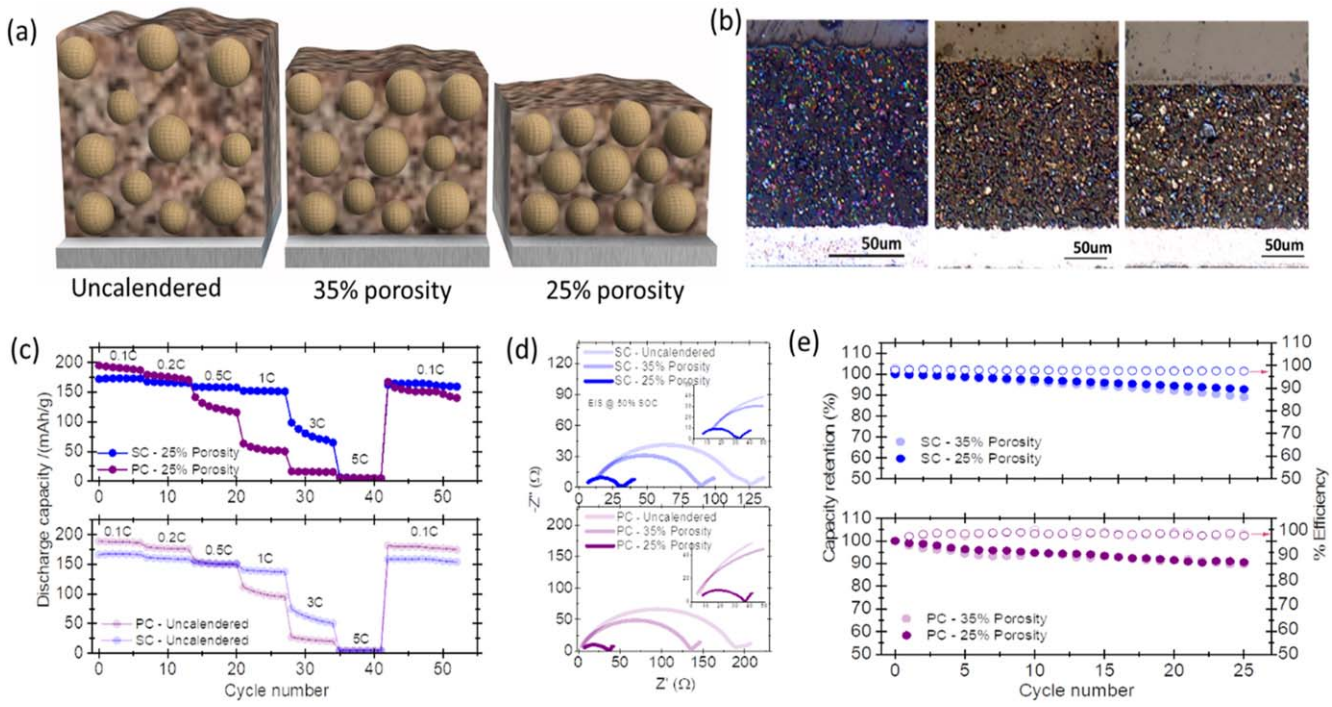

Figure 1. (a) Schematic illustration of electrode structures as a function of different degrees of compaction (uncalendered, calendered to 35% and 25% porosity). (b) Optical images of uncalendered and calendered to 35% and 25% porosity single crystal NMC811 electrodes. Half-cell electrochemical performance viz., (c) rate capability (d) Nyquist plots, and (e) cycle stability, comparing SC and PC electrodes as a function of different degrees of compaction.

process does not alter the electrochemistry of the cathode in any way at a slow rate (C/20). The PC and SC electrodes exhibited an initial capacity of 199 mAh g^{-1}, and 189 mAh g^{-1} regardless of the calendering density. The PC and SC electrodes have the same areal loading of 15 mg cm^{-2} and the formation cycles were all conducted at C/20 with cut-off voltages of 3.0 to 4.3 V.

Before carrying out detailed degradation studies, we verified how rate performance affects the capacity retention of PC and SC electrodes with different porosities. Figures 1c and S2 show that for SC electrodes, there is little change in C-rate performance as the packing density increases, however, for PC electrodes, the capacity drops off more rapidly as a function of C-rate in the case of highly

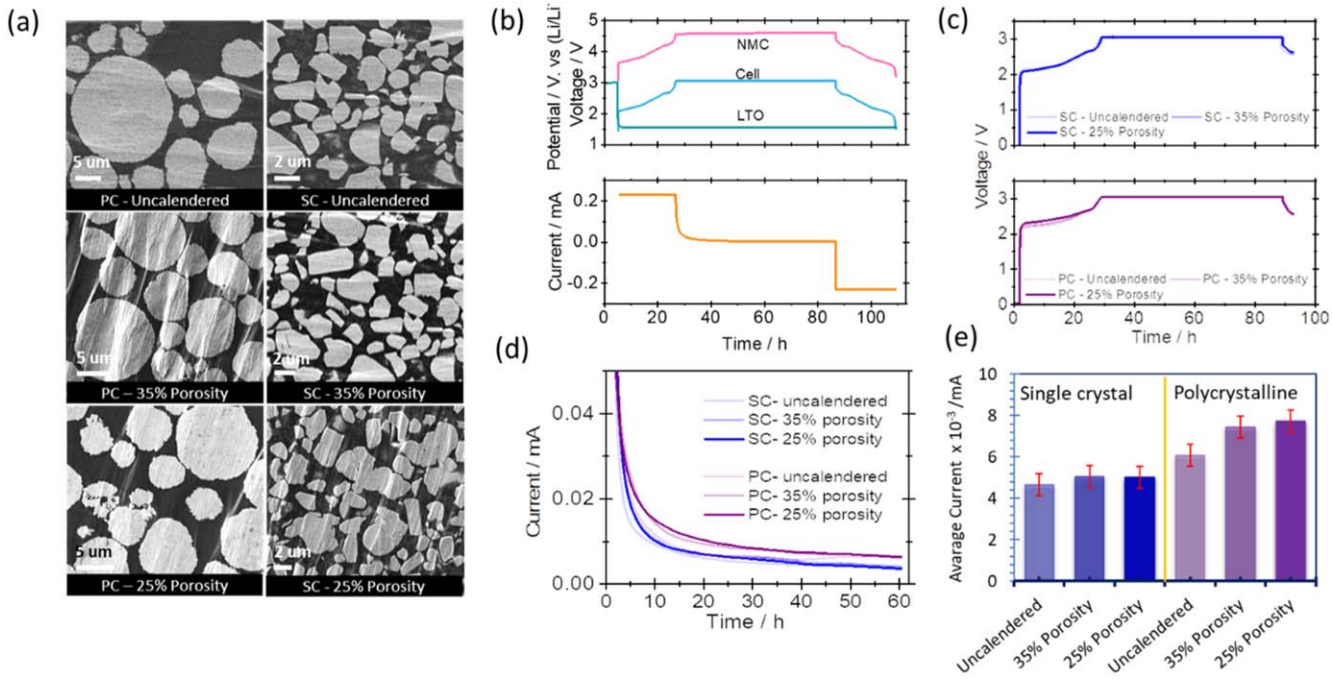

Figure 2. Surface properties of SC and PC electrodes with different degrees of calendering. (a) SEM cross-section images of uncalendered, calendered to 35%, and calendered to 25% porosities of poly and single crystal NMC811 electrodes. (b) Potential and current SC NMC811/LTO profiles in a three-electrode cell with a Li metal reference electrode. (c) Voltage profiles of PC and SC electrodes with varying porosities against LTO during the first charge-discharge cycle with a potentiostatic hold at 3.05 V vs Li/Li+ for 60 h. (d) Oxidation current observed during the potentiostatic hold. (e) The average current in the final 40 h hold for both PC and SC electrodes with varying porosities. The error bars in (e) depict the variability derived from two or more cells.

calendered electrodes. To understand where this difference comes from, we carried out electrochemical Impedance Spectroscopy (EIS) measurements in half-cells after formation cycles at 50% SOC (Fig. 1d). As the porosity decreases, the charge transfer (R_{ct}) resistance (mid-frequency) decreases for all electrodes. The R_{ct} values for the SC uncalendered electrodes and those compacted to 35% and 25% porosities are 105.7Ω, 79.3 Ω, and 32.2 Ω, whereas polycrystalline electrodes R_{ct} values are 184.8 Ω, 133.3 Ω, and 33.6 Ω, respectively. For SC electrodes we also found a systematic decrease in series (high frequency) resistance of 11.3, 9.5, and 4.1 Ω for uncalendered, 35% and 25% porosity respectively. In comparison, the polycrystalline electrodes show a series resistance of 6.6, 4.3 and 7.3 Ω. The increased PC contact resistance at 25% porosity might be due to cracking, resulting in poor contact with certain parts of the electrode (more evidence for cracking is provided further on). This could contribute to the poor rate performance observed in highly calendered PC NMC811 electrodes and explain why calendering densities for these electrodes typically does not exceed 35%. Figure 1e shows the half-cell cycling stability of both single-crystal and polycrystalline electrodes with varying porosities at a 1 C rate. Within the first 25 cycles, no significant difference was found in cycling stability as a function of calendering. Given the limited reliability of half cells for long-term cycling performance in high-loading cells, cycling stability in full cells against graphite anode are examined in later sections.

SEM cross-sections through SC and PC electrodes prepared with different porosities (Fig. 2a) showed limited differences in particle cracking under the imaging conditions used, except for the PC electrode with 25% porosity where some cracked particles are visible (Fig. 2a). It is however difficult to quantify the amount of cracking based on SEM cross sections as some nanoscale cracks may be too small to observe and higher cracking density occurs at the electrode surface compared to the bulk. As an alternative, we measured the amount of leakage current at a high voltage hold as a proxy of the amount of cathode surface exposed to the electrolyte. More specifically, we took our SC and PC cathodes with different porosities to a voltage of 3.05 V vs a lithium titanate (LTO) reference electrode for 60 h as shown in Figs. 2b and 2c (LTO is used because of its flat voltage profile and low reactivity with the electrolyte).[29] This corresponds to 4.6 V vs Li/Li^+ as confirmed by a 3-electrode measurement in Fig. 2b. Figure 2d shows that the current on the voltage hold decays rapidly within the first 20 h as the lithium-ion concentration in the cathode particles equilibrates. After this, the current stabilises rather than dropping to zero due to parasitic reactions, which are mainly due to electrolyte oxidation at the cathode surface.[20,29] The average current density during the last 40 h of the voltage hold is summarised in Fig. 2e. Given that the electrodes are using the same active material and the same areal loading, we assume in the first approximation that these parasitic reaction currents increase with the amount of wetted cathode surface area. PC electrodes showed increases in leakage current of 27% for highly calendered compared to uncalendered electrodes. In contrast, SC electrodes showed a much smaller increase in leakage current of about 7.6%, which indicates smaller increases in surface area when calendering SC compared to PC cathodes.

Next, GITT was used to investigate differences in lithium diffusion and resistance as a function of SOC for SC and PC electrodes with varying porosity. In our GITT protocol, constant current pulses of 20 mA g^{-1} (C/10) are applied for 30 min, followed by a 12 h rest period with no current passing through the cell and more information is provided in the supplementary note 1. As shown in Fig. 3, all electrodes show similar equilibrium potential irrespective of electrode porosity, as expected since the same active material is used. However, significant changes in overpotential are observed when changing the porosity. The uncalendered SC and PC electrodes both showed high internal resistance and low diffusivity in the charge and discharge processes. Interestingly, the PC electrode with 35% porosity showed a low internal resistance in both charge and discharge processes and a Li diffusivity comparable to the 25% porosity PC electrode (Fig. 3c). SC NMC811 electrodes with 25% porosity show lower internal resistance and higher lithium diffusivity in both charge and discharge processes than the PC electrode with similar porosity (Fig. 3c). Figure 3d shows that the overpotential of highly calendered 25% porosity PC electrodes is higher than that of SC electrodes. The observed higher internal resistance values of the 25% porosity PC electrodes further corroborate the rate performance and EIS analysis discussed in Fig. 1.

Next, full-cell studies vs graphite anodes were conducted to investigate the effect of calendering on battery cycling stability. Figure 4a demonstrates that higher levels of calendering result in substantially higher volumetric capacities due to a reduction in electrode thickness. In particular, cells with 25% porosity exhibited an almost 1.6-fold increase in the volumetric capacity of uncalendered cells. Throughout the cycling process, cells with both 35% and 25% porosity cathodes maintain higher specific capacities than uncalendered, even for the 25% porosity PC electrodes that have a higher surface area after calendering (Figs. 2a, 2e) and potentially more cathode surface reduction as a result.

The capacity retention after 300 cycles for PC electrodes is 62%, 63%, and 66% for uncalendered, 35% calendered, and 25% calendered porosity, respectively (Fig. 4a). In the case of SC electrodes, the capacity retention under the same conditions is 65%, 70% and 76% respectively (Fig. 4a). Every 100 cycles at 1 C rate, we carried out 3 diagnostic cycles at C/20 to decouple impedance losses from material degradation. After the initial 100 cycles at 1 C, the SC electrode with 35% and 25% porosity retained 82% and 86% of their initial specific capacity at C/20 (∼182.5 mAh g^{-1}) (Figs. 4b and 4d), while the uncalendered SC electrode retained only 63% specific capacity. Similarly, PC electrodes with 35% and 25% porosity retained 63% and 68% of their initial specific capacity (∼182.7 mAh g^{-1}), with the uncalendered electrode retaining only 61% (Figs. 4c and 4e). The lower capacity loss of the SC electrodes in the initial 100 cycles both with decreased porosity (increased calendering), and compared to the PC electrodes, is an indication of less impedance build-up in the cells in agreement with the EIS and GITT data discussed above, however, small variations in electrochemical data may occur depending on the source of materials used. It is worth noting that uncalendered electrodes experienced a more pronounced capacity loss during the initial cycles.

Hybrid pulse power characterisation (HPPC) was conducted with 55 mAh single-layer pouch cells (Fig. S3). The single-layer pouch cells were assembled with both SC and PC electrodes of 25% porosity against graphite anode. The heavily calendered 25% porosity SC electrode showed lower polarization growth than the PC electrode with similar porosity (Figs. 4f and 4g). Importantly, the PC electrode is unable to reach the full depth of discharge (DOD) investigated during pulsing after 200 cycles, and the resistance increases systematically over extended cycling.

In addition to the half-cell impedance measurements shown in Fig. 1, we carried out EIS measurements every 100 cycles at 50% SOC (Figs. 5a and 5b). Since the reduction of the cathode surface is known to be a major contributor to impedance buildup in NMC811-graphite cells,[30] the highly calendared PC electrodes which showed a clear increase in surface area suffer from faster impedance build-up. The 25% porosity SC electrodes show a nominal 12Ω upsurge in Rct values per 100 cycles (Fig. 5a), whereas their PC counterparts exhibited a more substantial increase of 100% (from 112Ω ∼210Ω R_{ct}) (Fig. 5b) for the initial 100 cycles. Although the overall impedance is lower at 25% porosity, it proportionally grows faster in the PC 25% porosity electrode than the PC 35% porosity which is about a 3-fold increase in 25% whereas a 2-fold increase in the case of 35%. This would be consistent with the higher surface area of the 25% PC electrode. Both

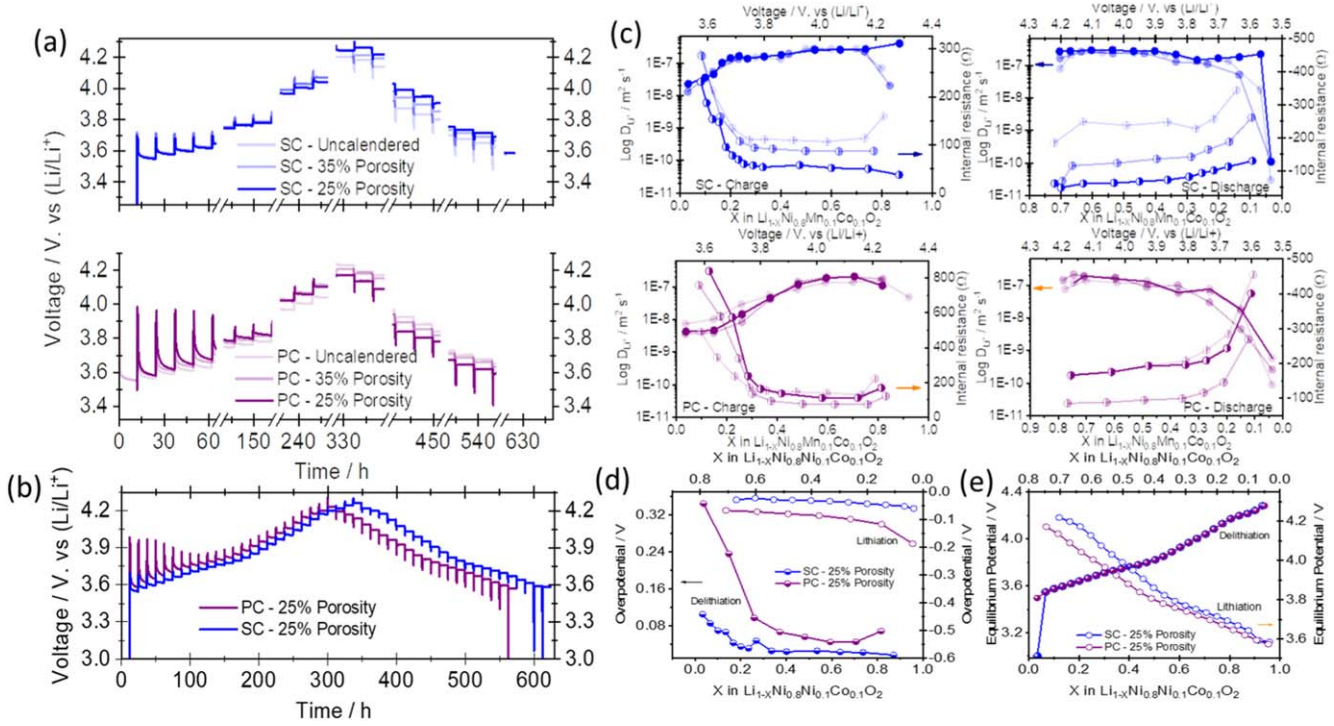

Figure 3. (a) GIIT profiles of SC and PC electrodes with varying porosity. (b) GIIT profile comparison of heavily calendered SC and PC electrodes with 25% porosity. (c) Calculated Li diffusion coefficient and internal resistance for all the electrodes as a function of SOC. (d) Overpotential comparison of SC and PC electrodes with 25% porosity, and (e) Equilibrium potential of SC and PC electrodes with 25% porosity as a function of SOC.

uncalendered SC and PC electrodes showed more than a 100% increase in Rct values during the initial 100 cycles and demonstrated an additional ~50Ω increment with subsequent cycles.

To evaluate the structural degradation of the electrode, post-mortem FIB-SEM analysis of the electrodes in the discharged state was carried out after 300 cycles to visualise crack distributions inside the PC and SC particles. Compared to the PC particles in uncycled electrodes of different porosities (Fig. 2a) it can be seen that the cycled PC particles have all developed internal cracking consistent with intergranular fracture of the primary particle grain boundaries. This increase in cracks inside the PC particles is in agreement with the increase in leakage current observed after formation in Fig. 2e, and this is a signature of oxygen loss from the cathode surface, which is known to accelerate the battery degradations.[20] In comparison, the FIB-SEM cross-sections of SC particles show no visible cracks for any calendering conditions even after 300 cycles (Figs. 5c and S4).

Conclusions

This work investigates the effect of calendering on the volumetric energy density, rate performance and cycling stability of PC and SC NMC811 cathodes. By calendering SC electrodes to a porosity of 25%, the electrode thickness is reduced from 100 μm to 70 μm (with an electrode density of 4.2 g cm^{-3}), resulting in a 1.6-fold increase in volume density. In the case of PC electrodes, we found that above a density of 35%, the electrodes crack substantially and suffer from a lower rate performance, suggesting that a porosity of about 35% as often reported for commercial electrodes, is optimal. However, in the case of the SC electrode, we found no evidence of excessive cracking or a substantial decrease in rate performance when calendering the electrodes to 25%. In fact, SC electrodes with 25% porosity achieved better capacity retentions compared to less densely calendered electrodes and also showed improved pulse-power performance. This suggests that these new types of battery particles can be calendered more aggressively, leading to a higher energy density without sacrificing cycling stability or power performance.

Experimental

Electrode fabrication.—The procured polycrystalline (PC) NMC811, $LiNi_{0.8}Mn_{0.1}Co_{0.1}O_2$ powder (MTI Corporation) and the single crystal (SC) NMC811 (Sinochem) were dried in a vacuum oven overnight before preparing the slurry. The slurry was made using a thinky mixture by combining NMC811, PVDF binder (Solef 6020), and Super P (Timcal) in a mass loading ratio of 90:05:05 and NMP as the solvent. The slurry was cast onto 16 μm aluminium foil using a doctor blade. The coated electrode was dried in a vacuum oven at 120 °C overnight, resulting in electrodes with a mass loading of approximately 15 mg cm^{-2} and a thickness of about 100 um. To achieve industrially relevant density, both the single crystal and polycrystalline NMC811 electrodes were calendered to around 35% porosity, while another set of electrodes was calendered to approximately 25% porosity. All electrodes underwent calendering in both forward and reverse directions using a heated two-roller hydraulic-driven roll press machine set to 80 °C, aiming to enhance the malleability of PVDF. The SC electrodes have 2.7, 3.5, and 4.2 g cm^{-3} densities for uncalendered, and calendered to 35% and 25% porosity, respectively. The PC electrodes have 2.23, 3.13, and 3.58 g cm^{-3} densities for uncalendered, and calendered to 35% and 25% porosity, respectively.

The porosity (ε) was calculated using the below equation.

$$\varepsilon = 1 - \frac{M\left(X_{NMC}/\delta_{NMC} + X_{PVDF}/\delta_{PVDF} + X_C/\delta_C\right)}{V}$$

where M and V represent the mass and volume of the electrodes, while X and δ denote the mass fraction and density of the NMC, PVDF, and carbon black components within the electrode.

The graphite anode slurry is composed of 91.7 wt% artificial graphite (Hitachi), 6 wt% PVDF, 2 wt% conductive carbon, and 0.3 wt% oxalic acid, which is cast onto a 20 μm copper foil using NMP as the solvent. The resulting anode sheet has a loading of ~9 mg cm^{-2}, corresponding to around 3.06 mAg cm^{-2} based on the graphite anode capacity of 340 mAh g^{-1}. Similarly, the $Li_4Ti_5O_{12}$, LTO anode is formulated by combining LTO, PVDF binder and Super P in a loading ratio of 87:8:5, cast onto 16 um aluminium foil

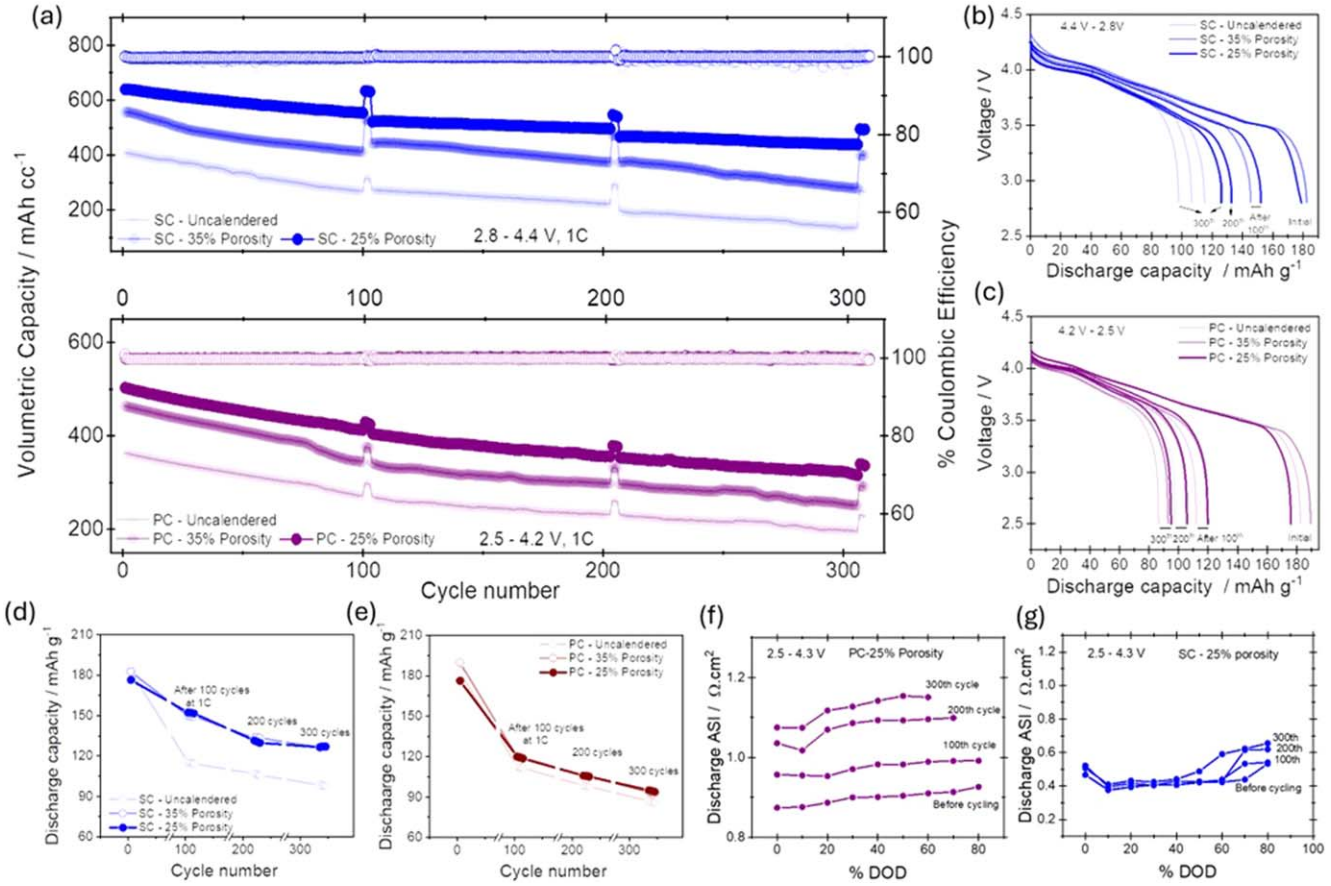

Figure 4. (a) The volumetric capacity of SC and PC electrodes with varying porosities against graphite electrode, cycle stability examined between 2.8–4.4 V for SC and 2.5–4.2 V for PC over 300 cycles at 1 C. Three recovery cycles at C/20 were conducted after every 1 C 100 cycles. (b), (c) The recovery discharge curves of SC and PC electrodes with different calendered porosity). (d), (e) Bar graph of the recovered capacity values from SC and PC electrodes with different porosities after different ageing cycles. (f), (g) HPPC results of both SC and PC electrodes with 25% porosity against graphite anode. ASI data is calculated as a function of the depth of the discharge.

utilizing NMP as the solvent. The LTO anode holds a loading of 23 mg cm^{-2}, compared to ∼3.68 mAh cm^{-2} based on the LTO capacity of 160 mAh g^{-1}. Electrode discs with diameters of 13 and 14 mm (cathode) and 15 mm (anode) are punched and subsequently dried at 120 °C for 12 h under dynamic vacuum before being transferred to an argon-filled glove box (with <0.5 ppm O_2 and H_2O, MBraun). The N:P ratio for electrode capacity balancing is set at approximately 1.1:1.0 for NMC vs graphite cells and ∼1.3:1.0 for NMC vs LTO cells.

Electrochemical cell assembly and protocols.—2032-type coin cells (CES, Cambridge) were assembled within an Argon-filled glovebox. Half-cells featured a 13 mm cathode, 15 mm lithium metal (Hohsen), and a 19 mm Celgard separator soaked in 42 μl LP57 electrolyte (SoulBrain). Full cells contained a 14 mm cathode, 15 mm graphite anode, and a 260 μm thick GF/B grade glass fiber separator soaked in 100 μl 1.3 M LiPF6 in EC: EMC: DEC (3:5:2 by Vol) with 9:1 wt% FEC, 0.5 wt% VC, and 0.2 wt% $LiBF_4$ (E-lyte Germany). After assembly, half cells underwent three formation cycles (CCCV, C/20, 3-4.3 V). Full cells were tap-charged to 1.5 V and rested for 10 h, followed by three formation cycles at C/20. Rate capability and cycle stability were assessed after these conditioning steps. All the electrochemical measurements were conducted in a climate chamber set at 26 °C. The potentiostatic holding test utilized three-electrode PAT cells (EL-Cell) with an 18 mm cathode and anode, a 260 μm thick glass fiber separator (GF/B grade) soaked in 100 μl of LP57 electrolyte (1 M LiPF6 in EC/EMC 3:7 vol%), and a lithium metal ring electrode in an insulation sleeve. Cells were galvanostatically charged at C/20 to 3.05 V (vs LTO) using Biologic VMP3 potentiostat, held at that voltage for 60 h with current monitoring, and then discharged at C/20 to 1.45 V. Electrochemical Impedance Spectroscopy (EIS) was carried out with the Biologic BCS 805 Series at 3.8 V and 10 mV amplitude and the scanning frequency spanned from 10 kHz to 10 mHz. Single layer pouch cells with the dimensions of 49 × 50 mm were assembled with heavily calendered electrodes against graphite anode with a Celgard separator soaked in 0.5 ml of E-lyte electrolyte. After the formation cycles, the pouch cells were charged to 4.3 V at C/2 current in preparation for the HPPC test. After reaching the higher cut of voltage, the cells were rested for 1 h before discharge to 10% depth of discharge (DOD) at C/2, a 10 s 3 C discharge pulse and C/2 charge pulse applied with 40 s rest time and this pulse sequence was repeated at 10% DOD intervals, with the intermediate discharge performed using CC at C/2 to obtain the potential-dependent impedance. The HPPC test was conducted before cycling and after every 100 cycles. Area squared impedance (ASI) values are calculated from the change in cell voltage during the current pulses, using the geometric area of the cathode for the calculation.[31]

Microstructural analysis.—Uncycled cathodes were mounted into epoxy resin, cured at room temperature, and microtomed using a Leica UC7 ultramicrotome. The microtomed electrodes were mounted into a Gatan PECS II broad ion beam miller and ion polished with Ar^+ ions for 1 h at 6 keV and 1 h at 5 keV using gun angles of 0° and a stage rotation speed of 6 rpm. Secondary electron SEM imaging was performed in an FEI Inspect F.

The cycled cathodes were washed using dimethyl carbonate and stuck onto an Al-stub using carbon tape for focused ion beam

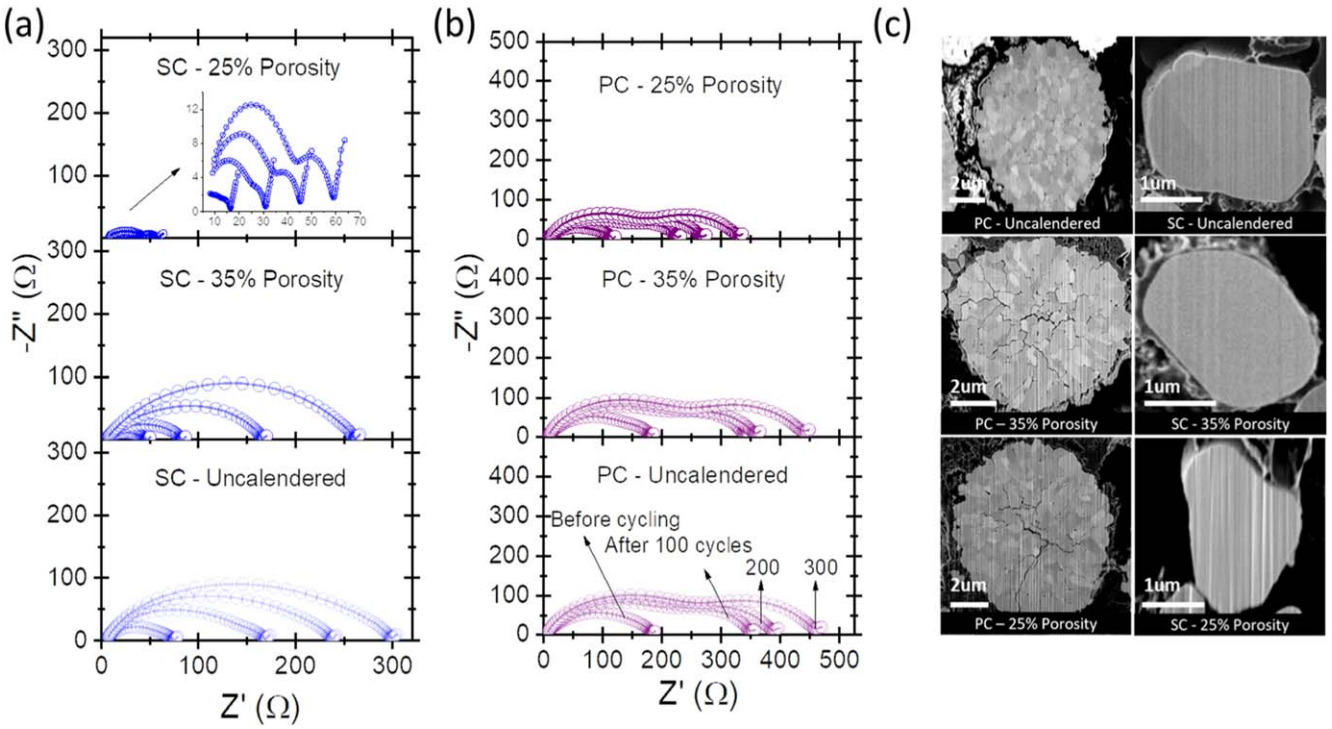

Figure 5. EIS spectra of uncalendered and calendered to 25% and 35% porosity electrodes, the cell impedance measured after the formation cycles at C/20 and after every 100 ageing cycles. (a) SC electrodes, (b) PC electrodes. (c) FIB-SEM cross-section images for SC and PC cathodes with varying porosities measured after ageing to 300 cycles at a 1 C rate.

scanning electron microscopy (FIB-SEM) experiments. These samples were stored in an argon glove box and then transferred to a Zeiss CrossBeam 540 dual beam Ga^+ FIB-SEM microscope to carry out cross-sectional imaging of the cathodes. A protective layer of Pt (1 μm thick) was deposited over an area of 20 μm × 30 μm. Initial FIB rough milling was carried out using a 30 nA Ga-ion beam current at 30 kV to prepare a 20 μm × 30 μm × 30 μm volume, and then cross-sectional slices of about 50 nm in nominal thickness were removed using a 1.5 nA Ga ion beam at 30 kV. A secondary electron image was acquired after each slice using a 2 kV accelerating voltage and 1.1 nA beam current.

Acknowledgments

The authors acknowledge the financial support received from the Faraday Institution project (FutureCAT- FIRG017 and FIRG065). MDV also acknowledges support from the European Research Council (ERC Consolidator Grant - MIGHTY 866005). MDV, AM, MCL and CD acknowledge the Faraday Institution (Degradation project grants - FIRG001 and FIRG024) for funding the focused ion beam milling work.

ORCID

Kumar Raju https://orcid.org/0000-0002-6143-0720
Laura Wheatcroft https://orcid.org/0000-0003-2306-9791
Louis F. J. Piper https://orcid.org/0000-0002-3421-3210
Beverley J. Inkson https://orcid.org/0000-0002-2631-9090
Michael De Volder https://orcid.org/0000-0003-1955-2270

References

1. K. Turcheniuk, D. Bondarev, G. G. Amatucci, and G. Yushin, "Battery materials for low-cost electric transportation." *Materials Today*, **42**, 57 (2021).
2. R. Schmuch, R. Wagner, G. Hörpel, T. Placke, and M. Winter, *Nat. Energy*, **3**, 267 (2018).
3. Z. P. Cano et al., *Nat. Energy*, **3**, 279 (2018).
4. R. Sim, S. Lee, W. Li, and A. Manthiram, *ACS Appl. Mater. Interfaces*, **13**, 42898 (2021).
5. E. N. Primo, M. Chouchane, M. Touzin, P. Vazquez, and A. A. Franco, *J. Power Sources*, **488**, 229361 (2021).
6. H. Zheng, L. Tan, G. Liu, X. Song, and V. S. Battaglia, *J. Power Sources*, **208**, 52 (2012).
7. R. Ge, D. J. Cumming, and R. M. Smith, *Powder Technol.*, **403**, 117366 (2022).
8. D. Schmidt, M. Kamlah, and V. Knoblauch, *J. Energy Storage*, **17**, 213 (2018).
9. D. Schreiner, M. Oguntke, T. Günther, and G. Reinhart, *Energy Technology*, **7**, 1900840 (2019).
10. T. M.-M. Heenan et al., *Adv. Energy Mater.*, **10**, 2002655 (2020).
11. E. N. Primo, M. Touzin, and A. A. Franco, *Batter Supercaps*, **4**, 834 (2021).
12. G. Lenze et al., *J. Electrochem. Soc.*, **164**, A1223 (2017).
13. I. Bloom et al., "An accelerated calendar and cycle life study of Li-ion cells." *Journal of Power Sources*, **101**, 238 (2001).
14. B. L. Trembacki, D. R. Noble, M. E. Ferraro, and S. A. Roberts, *Journal of Electrochemical Energy Conversion and Storage*, **17**, 041001 (2020).
15. X. Lu et al., *Joule*, **4**, 2746 (2020).
16. S. G. Lee and D. H. Jeon, *J. Power Sources*, **265**, 363 (2014).
17. M. Jiang, D. L. Danilov, R. A. Eichel, and P. H.-L. Notten, *Adv. Energy Mater.*, **11**, 2103005 (2021).
18. S. Lee et al., *Adv. Energy Mater.*, **11**, 2100858 (2021).
19. J. K. Morzy et al., *ACS Appl. Energy Mater.*, **7**, 3945 (2024).
20. W. M. Dose et al., *ACS Energy Lett.*, **7**, 3524 (2022).
21. S. Lee, L. Su, A. Mesnier, Z. Cui, and A. Manthiram, *Joule*, **7**, 2430 (2023).
22. S. Jie Lu et al., *Electrochemical Energy Reviews*, **5**, 15 (2022).
23. J. Langdon and A. Manthiram, *Energy Storage Mater.*, **37**, 143 (2021).
24. X. Fan et al., *Nano Energy*, **70**, 104450 (2020).
25. H. H. Ryu, S. B. Lee, C. S. Yoon, and Y. K. Sun, *ACS Energy Lett.*, **7, 9**, 3072 (2022).
26. J. C. Stallard et al., *J. Electrochem. Soc.*, **169**, 040511 (2022).
27. L. Wheatcroft et al., *Batter Supercaps*, **6**, e202300032 (2023).
28. J. C. Stallard et al., *Joule*, **6**, 984 (2022).
29. W. M. Dose et al., *ACS Appl. Mater. Interfaces*, **14**, 13206 (2022).
30. W. Weppner and R. A. Huggins, *J. Electrochem. Soc.*, **124**, 1569 (1977).
31. W. M. Dose, C. Xu, C. P. Grey, and M. F.-L. De Volder, *Cell Rep. Phys. Sci.*, **1**, 100253 (2020).